Ilorin Journal of Science
Volume 3, Number 1, 2016, pp. 11 – 26 (Printed in Nigeria)
ISSN: 2408 – 4840 © 2016 Faculty of Physical Sciences, University of Ilorin
https://doi.org/10.54908/iljs.2016.03.01.002

ILORIN
JOURNAL OF SCEINCE

ILJS-15-067

Reflection Enhancement Processing in Ultra-Shallow Seismic Data

Raji*, W. O.

Department of Geophysics, University of Ilorin, PMB 1515, Ilorin, Nigeria.

Abstract

The lack of standard procedure for processing shallow reflection seismic data is an impediment to the use of reflection seismic data for near surface applications. The wave field of ultra-shallow reflection data is often complicated by low frequency high amplitude events in the same time window with primary reflections. The standard method for processing exploration-scale seismic data proved unsatisfactory for ultra-shallow reflection seismic data: scaling down the acquisition geometry is inadequate because the frequency bandwidth of the data recorded does not scale up in the same proportion. In this study, data-driven workflow of specialised techniques is used to preserve the low-amplitude energies reflected by shallow geological layers. Surgical top and end muting; cone and polygonal muting; $\boldsymbol{f-kx}$ spectral-filtering techniques and careful validation of coherent events, by synthetic modelling, were combined to degrade noise and other non-reflection events. A combination of constant velocity gather, Semblance Plot, and Constant Velocity Stack techniques was applied to obtain the optimum move-out velocity. Applied to an ultrashallow seismic data from Southeast Spain, the workflow improved the signal-to-noise ratio of processed data. The CDP–stacked image constructed for the survey reveals some shallow vertical faults suspected to be associating with the main Carbonera Faults. These faults are comparable to faults projections constructed from a field based geological mapping undertaken many years before the seismic survey.

Keywords: shallow seismic survey, reflection processing; noise attenuation, velocity analysis, CDP-stacking.

1. Introduction

In shallow seismic data acquisition, energy sources are usually placed at few metres below the receivers' level in the weathered and unconsolidated layer. The strong velocity variation within the weathered layer where the sources are placed is a known source of error in travel time analysis of shallow seismic data. In addition to this, non-reflection arrivals like ground roll, airwaves, and direct arrivals in shallow seismic data have unique characteristic due to strong velocity perturbation, and they are somewhat different from the noise observed in exploration seismic data where the target layers may be hundreds of metres below the source.

*Corresponding Author: Raji, W. O.
Email: wasiu.raji@gmail.com, lanreraji@unilorin.edu.ng

Comparison between seismic data used for oil and gas exploration and shallow seismic reflection used for near surface engineering and groundwater studies suggests reciprocity of methodologies for reflection processing. But, processing shallow seismic reflection data is different from processing exploration-scale seismic data (Baker *et al*., 1998, Miller, 1992, Black *et al*., 1994). It is not a simple scale-down of the method used for processing oil and gas exploration seismic data. Geological–model driven techniques must be applied to correct travel time error arising from the velocity variation in the shallow weathered zone.

Successful processing of very shallow seismic reflection data requires careful validation of reflections events to distinguish true reflections from coherent noise presenting themselves as reflections. This validation requires good knowledge of the behaviour of waves reflected, refracted, or diffracted at a distance very close to recorders and synthetic seismic modelling of different wave modes. Errors introduced by incorrect velocity analysis and inappropriate static correction can lead to artefacts that may line-up like reflections on CDP stacked image, thereby misleading seismic interpreter when interpreting the stacked section (Steeples and Richard, 1998). Inappropriate static correction, non-vertical incidence, and source receiver variability can lead to frequency degradation of reflection wavelets when going from Common Shot Gather to Common Depth Point gather (Gruber and Rieger, 2003). The wave field of shallow seismic data is complicated by near source noise arriving within the same time-offset window of reflection arrivals. A combination of these problems often lead to poorly signal-to-noise ratio that are unlikely to yield interpretable and geologically plausible structures.

The acquisition geometry for shallow reflection survey is different from that of exploration scale reflection survey. Acquisition of shallow seismic data requires denser sampling, in terms of space and time, compare to normal seismic data (Gruber and Rieger, 2003). Processing this data required some model predicted techniques that can suppress the unwanted signal with no damaging consequence to reflections. Purely scaling down the acquisition geometry is inadequate because the frequency bandwidth of the data recorded does not scale up in the same proportion (Evison, 1952; Hover and O' Brien, 1980; Raji and Rietbrock, 2013).

Although seismic refraction has been successful for groundwater studies, the shortcomings of the methods include: the difficulty in discriminating true refraction from direct arrival at large offset; the requirement to have offset twice the depth of layer to be investigated limited

seismic refraction application in developed residential areas where space is limited; and the problem of hidden layer limited refraction application in the basement complex where the aquifers are found at great depth, and have limited and irregular extent. Seismic reflection method does not require an offset that is twice the depth to be investigated, reflections have characteristic hyperbola (move out) that distinguish them from other events. But processing shallow reflection is still a problem because the existing methods are developed for exploration-scale seismic data.

The goal of this paper is to describe some specialised techniques required to: (i) process shallow seismic data to optimally enhance the shallow reflection arrivals and suppress other non-reflections wave modes, and (ii) image the data to reveal the near surface structural features in the study area. These techniques include static corrections, surgical top-end muting, polygonal and cone muting, High –pass filtering, $f-k$ spectral filtering, semblance velocity analyses, and CDP stacking.

The techniques are demonstrated using a data set acquired at shallow depth along the narrow zone of the Carbonera fault, Southeastern Spain (Fig. 1a). The survey lines covered a total length of about 1.5km. Carbonera fault is a part of a large fault system that cuts across the southern margin of the Iberian Penisula (Faulkner *et al.*, 2003). Due to erosion, the faulted mica schist basement rock is exposed at the surface in some places. The faults aided weathering of the exposed rock. The Carboneras fault system cuts all the basement rocks plus the volcanic units and almost all the components of the post-orogenic sedimentary rock sequence, although progressively younger rocks are less affected by the faulting. The Carbonera Fault Zone (CFZ) in the basement rocks consists principally of two strands of fault rock, respectively, the northern and southern strands of the CFZ, with subsidiary fault strands between them (Faulkner et al., 2003; Rutter et al., 2012). The two bounding faults enclose a tract of significantly higher grade basement schists, bearing staurolite, andalusite and sillimanite, locally migmatitic with minor granitoids that yielded ~ 20 Ma ages (Platt and Whitehouse, 1999). The outline geological map of the Carbonera Fault Zone is shown in Figure 1b.

2. Data Acquisition

High resolution shallow seismic experiment was undertaken at El Saltador, a community lying along the narrow zone of the Carbonera fault system, South-eastern Spain (Figure 1a) in 2012. The goal of the survey is to delineate the Carbonera fault zone believed to exist in this area. The experiment consisted of four survey lines totalling about 1.5km (about 1km on a straight line) running approximately north to south, terminating in El Saltador village (Fig. 2). A total of 77 explosive sourced shots were fired at 14m interval intervals. Each shot comprised 168 or 192 geophones with 2m spacing. Shot and receiver distances were recorded in the observer logbook, while the coordinate description and the elevation of each geophone and the shot peg were acquired using Surveyor's Geographic Positioning System. Prior to data acquisition, trial tests were done at every shot point to ascertain the suitability of the survey design. Following the trigger test, the explosive source is shot at designated positions, one after the other. Seismic arrivals are recorded by the geophones positioned along each of the four survey lines. The shots produced strong non – reflective events that dominate the field records. A representative raw data is shown in Figure 3.

3. Seismic Processing

3.1 Geometry and Static Application

The four survey lines were combined into a single seismic line covering a horizontal distance of about 1.5km as shown in Figure 2. The combined line consists of a total of 77 shots. 76 out of the 77 shots were processed. One of the shots could not be processed because it does not contain any useful data. A typical example of the field record is shown in figure 3. The data set is processed using commercial software, Globe CLARITAS. To begin processing, observer's file and surveyor's record were merged to create a geometry database. The geometry database is then added to the trace headers. The trace length was reduced to 1500ms from 4000ms having confirmed that no useful information is present beyond 1500ms. First break time picking was done using both automatic and manual process. Automatic process was done at first-pass to save time, while manual process was done to correct the errors in the automatic picks. Figure 4 shows the time picks for each trace. Each first-break pick contains two essential information which are the travel time and distance.

These information are essential in the determination of velocity. Hence accurate first-break picking is important for velocity estimation and seismic imaging.

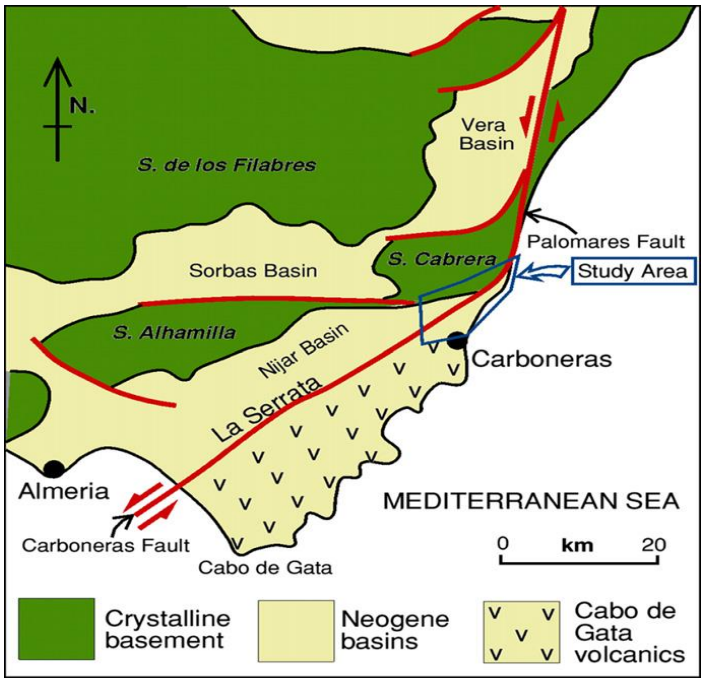

Figure 1a: Outline map of SE Spain showing the disposition of uplifted basement blocks (Sierras) and the Neogene sedimentary basins that are often bounded by major faults. La Serrata is a topographic ridge of intrusive igneous rocks that outcrops for about one-third the length of the onshore outcrop of the Carboneras fault, Rutter *et al*., 2012.

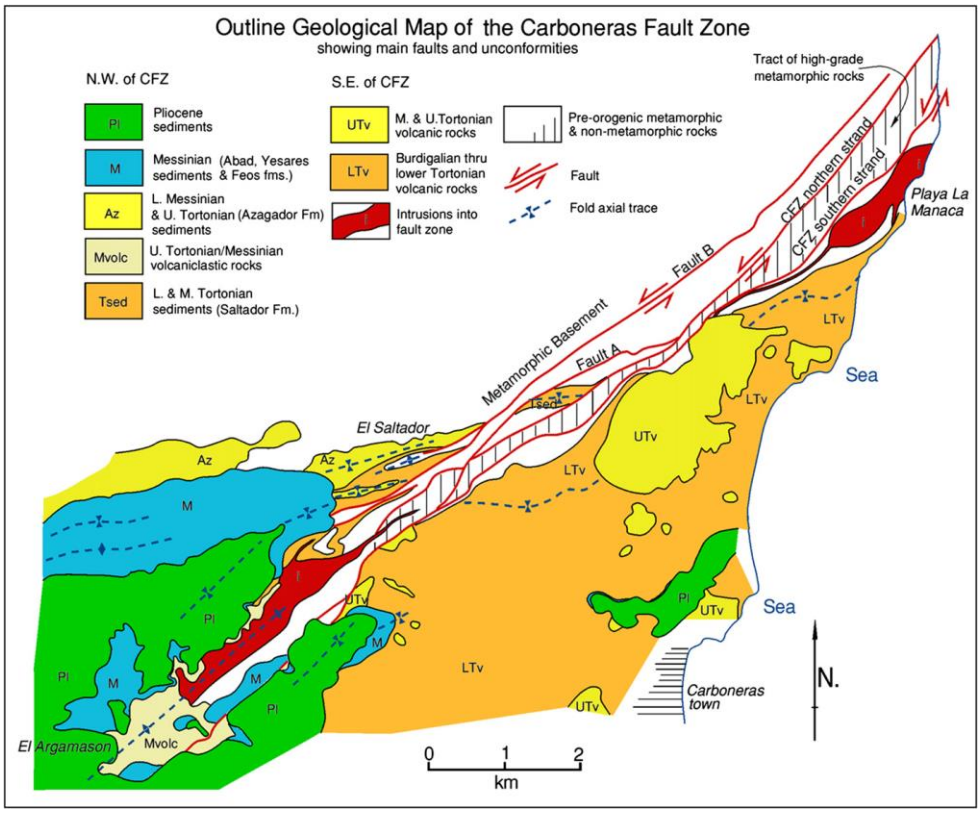

Figure 1b: Outline geological map of the CFZ, in which the area is divided into units defined by principal faults and unconformities (Rutter *et al*., 2012).

Figure 2: Satellite map of the study area showing the survey profile and geophone arrangement.

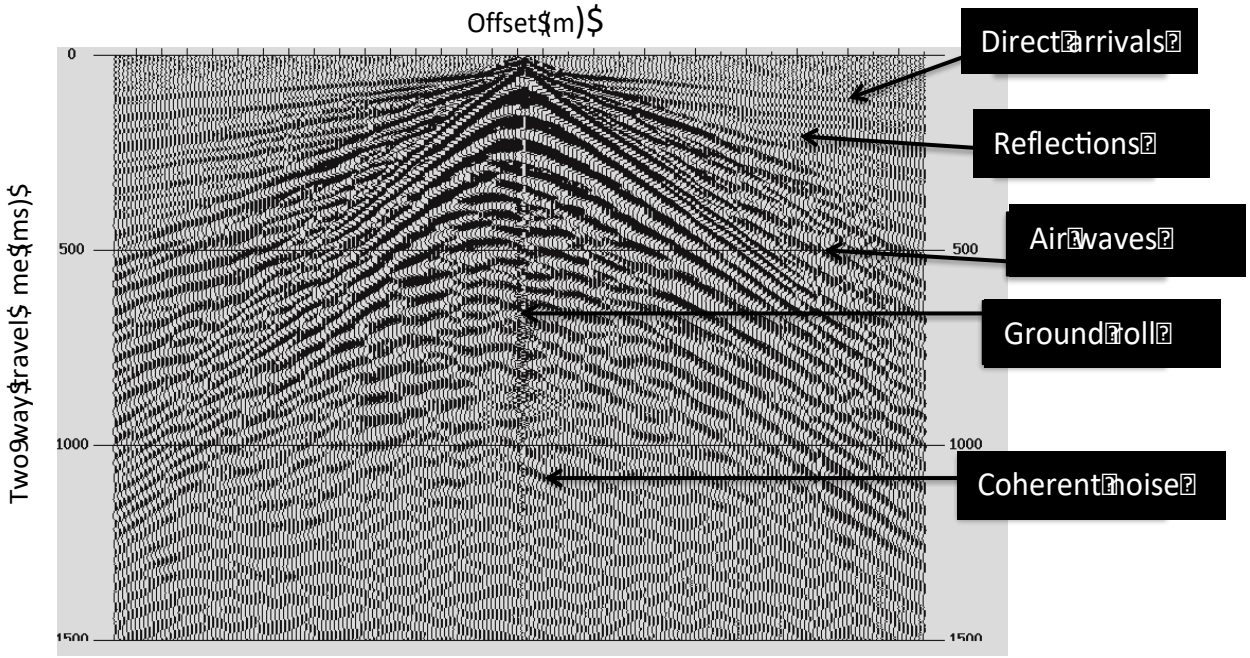

Figure 3: A representative shot gather. Shot 9 of 77 showing some of the wave modes identified in the data.

The first arrival travel times were analysed to produce a 2D earth model (velocity and depth) that was used to calculate the surface consistent static shift. Static shift was applied to each shot/receiver to correct the data for spurious velocity and topographic effects. Near surface spurious velocity effect arise from variation in weathered zone thickness and topography at the shot-receivers location. For complex velocity perturbations in the weather layer, a velocity tomography method using geological priory (Raji *et al*., 2016) will be necessary. The overall effect of static correction is to 'replace' the unconsolidated upper layer with a constant velocity medium. The static application processes consists of five iterations per run. The process was discontinued when the lowest possible RMS error was obtained. The RMS error is the misfit between the picked first-break time and the theoretical times generated (by ray tracing) through the earth model. Datum statics was performed to correct for elevation difference between the two ends of the survey line (102.50m and 121.00m). The consequent effect of datum statics shifted the source and receiver to a flat constant datum (125m). The two statics files were applied to the raw data containing geometry database.

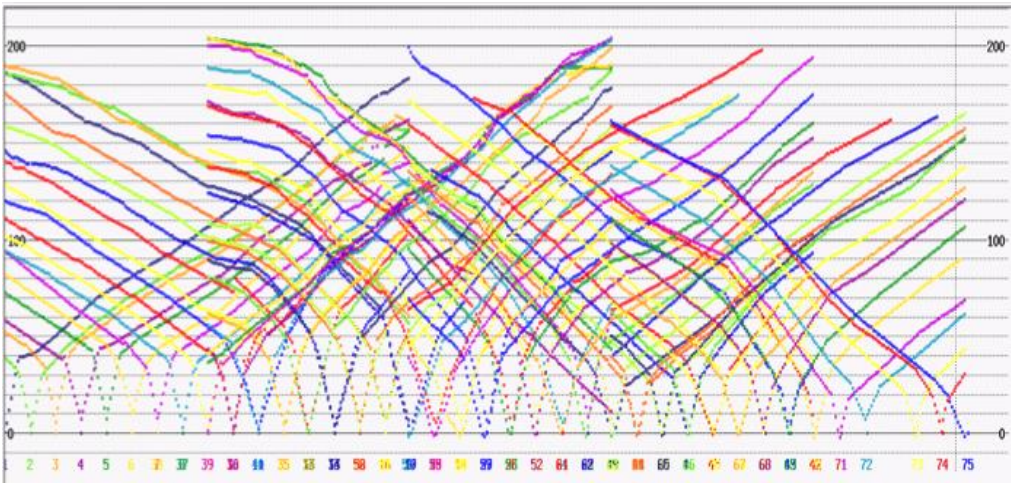

Figure 4: Travel time picks for the first arrivals. Each of the 168/192 dots per shot represents one first break pick. The picks are coded by the shot-numbers.

The correction for elevation statics and spurious velocity in weathered zone are defined in equations (1 and 2) as written below:

$$\Delta t = \frac{h_s}{v_1} - \frac{h_r}{v_1}, \qquad (1)$$

$$\Delta t = \left[\frac{v_1 - v_a}{v_1 v_a}\right] h_a \,, \quad (2)$$

where Δt is the time shift to be applied to the traces, h_s is the height above the datum, h_r is the height below the datum, h_a is the thickness of the weathered zone, v_1 is the velocity of the weathered zone, v_a is the spurious velocity in the weathered zone.

3.2 Wave modes analyses, trace editing, and noise suppression

Careful visual inspection of each shot gather showed that the shots produced strong ground roll and air waves which dominate the field record thus making reflection arrivals very difficult to identify. Velocity function ruler, F-K spectrum (dip), and frequency characteristic modules in Globe CLARITAS were used to analyse the traces, from one gather to another. Apparently, the shallow part of the data consists of refractions, some reflections, and direct arrivals. Ground rolls marked with high amplitude and low frequency (forming pseudo-hyperbolic features) dominates the deeper portion of the data. Noisy traces were removed through surgical muting by setting their amplitude and frequency to zeros. Before trace editing, various band-pass filters and high pass filters were tested with the data to determine the best frequency range that can be used to discriminate reflections from non-reflection arrivals during filtering. Further to this, the data set was sorted to Common Depth Point to have first-hand information of where reflections hyperbolas may be found, and to help decide what method would be best to get rid of noise and other non-reflection arrivals.

Surgical top muting was applied to remove direct arrivals and refractions, while a polygonal mute technique was used to remove air waves and the ground rolls that may not be suitably removed by $f - kx$ muting or frequency filtering. In all muting process, the amplitude of the noise is set to zero and the portion of the data where muting is to be applied is described with time and space or trace number. Non-reflection events found in the same time–spaces with the reflections are suppressed by high-pass filter in frequency-wavenumber domain (Haberland *et al*., 2007 and Maercklin *et al*., 2005). Any signal below 10Hz is filtered and the data is tapered in Fourier domain to prevent spectral smearing. The data output after this processing stage is shown in Figure 5. To circumvent the undesirable effects of spectral leakages due to polygonal frequency filtering, a combination of automatic gain correction (AGC), tapering, and un-AGC was applied. This method was found to be very efficient at

suppressing artefacts that are often introduced by frequency smearing and spectral leakages. Following this, a band-pass (10-12 – 25-30 Hz) filter is applied to remove wave modes with extreme frequencies.

Finally, another polygon muting is applied to remove all the waves below the reflection arrivals. Although some reflections are found in the same time-space where polygon muting was applied, they are believed to be multiples-reflections. Synthetic modelling of reflections and their multiples show that these events are multiple arrivals since the reflecting layer is at shallower depth (Raji *et al*., 2015). A CDP stacked image containing these reflections is less resolved than the final stack image. Figure 6 shows Common shot gather 9 after suppressing noise and non-reflection arrivals. The wave-field is now clearer and reflection events became easy to identify. The data set, after this stage, was passed on to the velocity analysis stage.

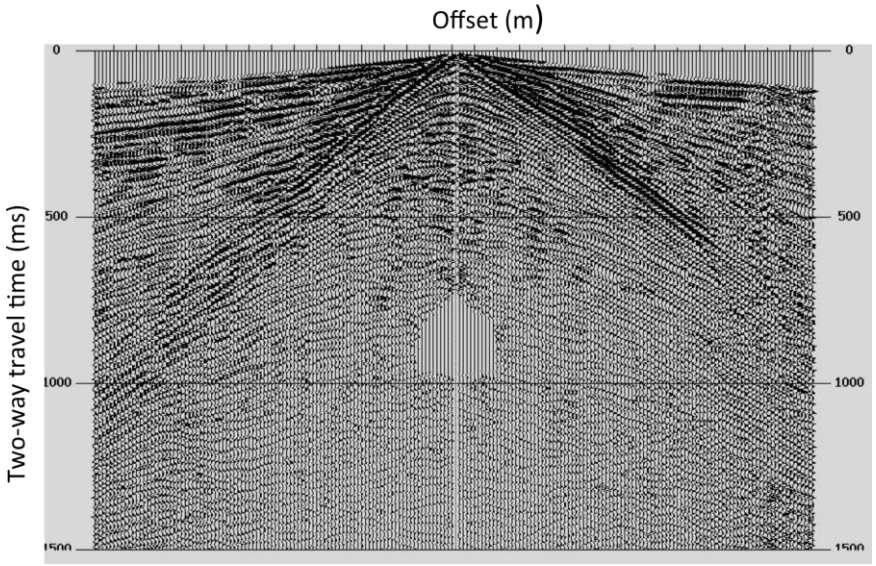

Figure 5: Common Shot Gather 9 of 77 partly processed to remove some refractions, direct waves, and low frequency wave modes at the top of the data.

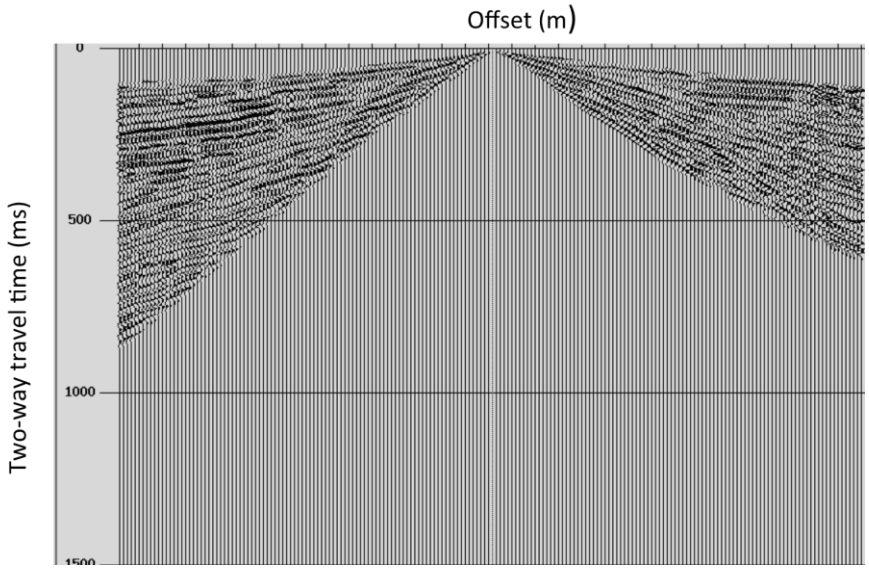

Figure 6: Fully processed field records for shot 9 of 77. Non-reflection arrivals have been optimally suppressed; reflections are now enhanced.

3.3 Velocity Analysis and Common-Depth-Point Stacking

Before velocity analysis, traces were sorted to Common Depth Points (CDPs). The number of traces in a CDP varies: they are fewer at the low CDP numbers, reaching maximum at the middle CDP numbers, and decreasing toward the high CDP numbers. The process of velocity analysis is essentially a forward modelling approach–matching the travel time picks to the model predicted travel times. To begin, an educative guess - a trial-by-error method is used to determine the starting velocity (Yilmaz, 1980; Baker *et al*., 1998). The model velocity that gave the best match and the least RMS error is taken as the true velocity. This velocity is used to stack the CDP-sorted traces.

The CDP-sorted traces are inspected for true reflection hyperbolas. At this point, caution was taken not to mistake hyperbolas formed by non-reflections arrivals (e.g. ground rolls) for reflection hyperbolas. To avoid this mistake, refection arrivals forming hyperbola in CDP gathers were traced back to the common shot or common receiver gathers. Those found to be true hyperbolas were fitted with curves (Figure 6) to estimate the Move-out velocity, NMO-velocity. The velocities determined by the curve-fitting method and the corresponding depths of the hyperbola were used as the input parameters to the velocity analysis. At near surface, adjustment for NMO on shallow reflection data is complicated by low signal-to-noise ratio and lack of strong reflection arrivals at near offset.

A combination of three methods: Constant Velocity Gather (CVG), Semblance Plot (SP), and Constant Velocity Stack (CVS) was used to determine the best stacking velocity. Velocity analysis starts with CVG method, continues with SP method, and ends with CVS. The velocity analysis continues until velocities that flatten or align the reflection hyperbolas were obtained. Because the data size is small, Continuous Velocity Spectrum (CVS) method was applied for final velocity analysis. A velocity step within the gradient of 3m/s to 5m/s was used for the CVS method. For this data, using higher velocity gradient in CVS degraded the spectral properties of the reflection wavelet and introduced high frequency artefacts. Except for speed, CVS is an efficient method for final velocity analysis because it allows a complete view of the entire CDP plots, thus allowing seismic processors to achieve maximum line–up and coherent reflections over reasonable distance while perturbing the input velocity. Reflection wavelets on seismic data were adjusted for non-vertically incident ray path before stacking the traces. A stacked image of the processed traces is shown in Figure 7.

4. Discussion

Considering the wave mode diversity and the characteristics of near source noise arriving within the same time-offset window with the primary reflection arrivals, the use of specialised techniques other than those used for conventional seismic processing became necessary. The core of the processing is driving by synthetic modelling by which true primary reflections are validated. Reflection enhancement in the ultra-shallow reflection seismic processing methods is data-driven aimed to enhance reflection arrivals and suppress other wave modes. The sequence of data processing applied in this study includes: geometry data application; visual inspection and Quality control; static and spurious velocity correction, wave field analysis and synthetic modelling; first arrival picking; trace editing; noise analyses and noise attenuation; Velocity analysis, semblance picking; CDP sorting; and CDP stacking.

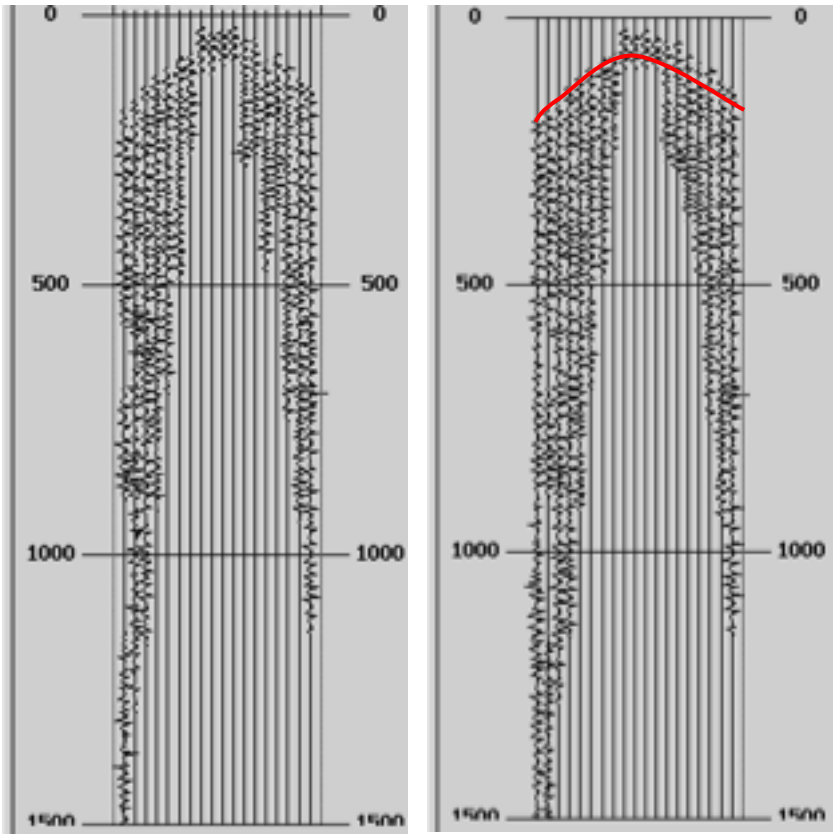

Figure 7: CDP 304 (left) and 324 (right) showing reflections hyperbolas. Curve is fitted to a reflection hyperbola in CDP 324 to determine NMO

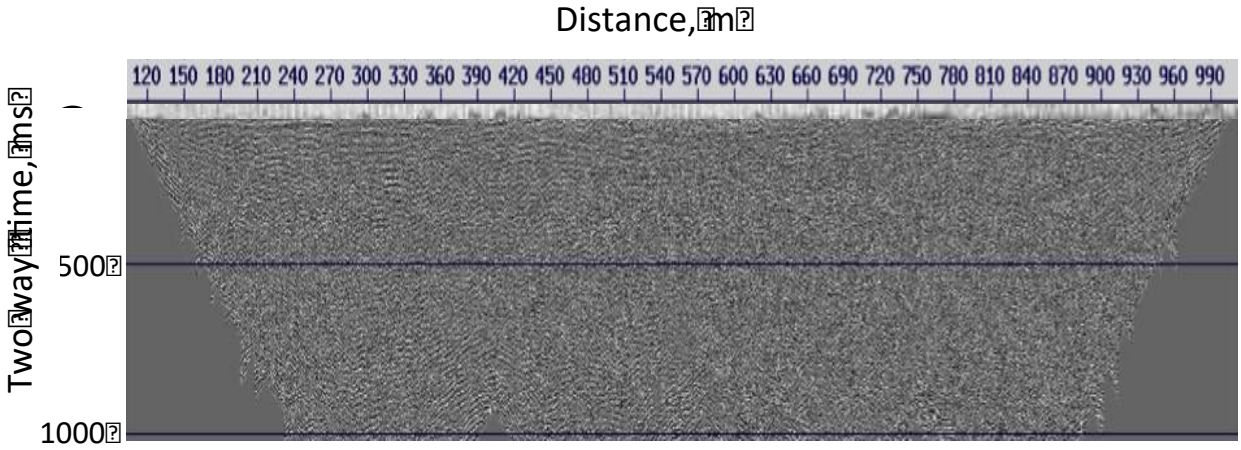

Figure 8: CDP-stacked image of the processed data plotted in variable density format.

For the noise attenuation process, a conservative surgical end mute was applied to remove refraction events. Noise cone muting was engaged to remove ground rolls and air waves contaminating the deeper section of the data (Baker, 1998; Haberland *et al*., 2007)). A band-pass filter (10-12 – 25-30 Hz) was used to remove non-reflective events present in the remaining section of the data. Conservative top shallow muting was applied to remove refractions arrivals in the top 80ms as it is not likely that true reflections may be found at this time interval.

However, the location of the reflecting interface between the basement rock and the overlying unconsolidated weathered material as shown in the stacked section (Figures 9 and 10) is further confirmed by synthetic modelling using velocities and depth determined from the first arrival picks. The stacked image is compared to various processing stages including the raw data, partly processed shot records, and pre-stack CMP gather to ascertain the originality, or otherwise of structures in stacked image. Since there is no evidence of dipping structures, the stacked image was not migrated. Vertical faults lines striking northwest – southeast direction were delineated on the seismic sections. These faults are found in the mica-schist (basement rock) underlying the unconsolidated layer. Some exposed section of the mica-schist show that the basement rock is weathered in some places. The weathering is probably aided by the vertical faults allowing water to penetrate the basement rock.

The similarity in the acoustic impedance of the unconsolidated layer and the weathered (Mica-schist) explains the absence of strong interface between the unconsolidated layer and the weathered basement rock. Deciphering the interface is aided by synthetic modelling using higher acoustic contrast. Overall, the faults delineated in the stacked section within weathered basement rock are comparable to the faults projections drawn from surface geological mapping undertaken many years before the shallow seismic survey. The processing techniques are generic and could be applied, with slight modification, to other shallow seismic data to study near surface geological structures and for groundwater and engineering applications.

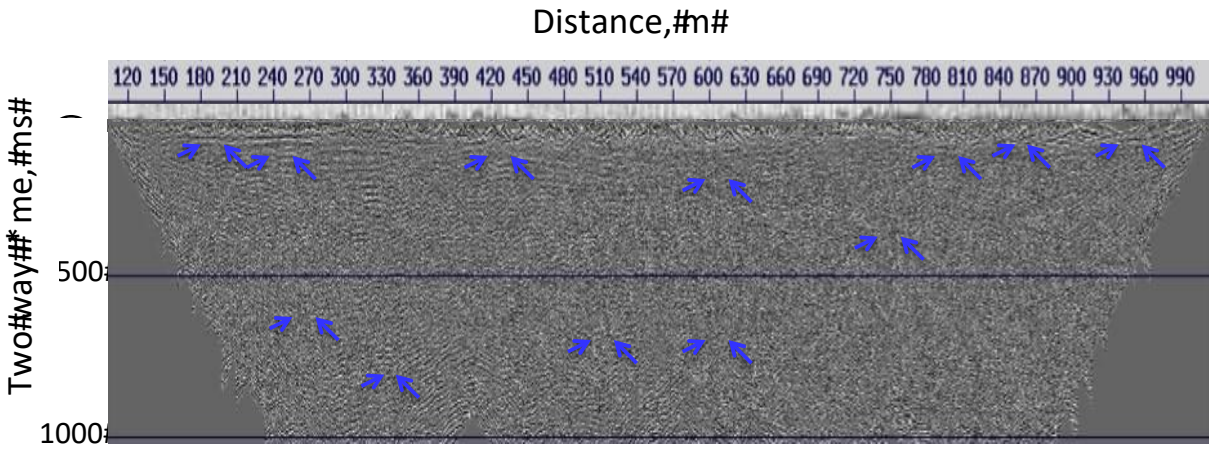

Figure 9: Qualitative delineation of fault lines on the CDP-stacked image

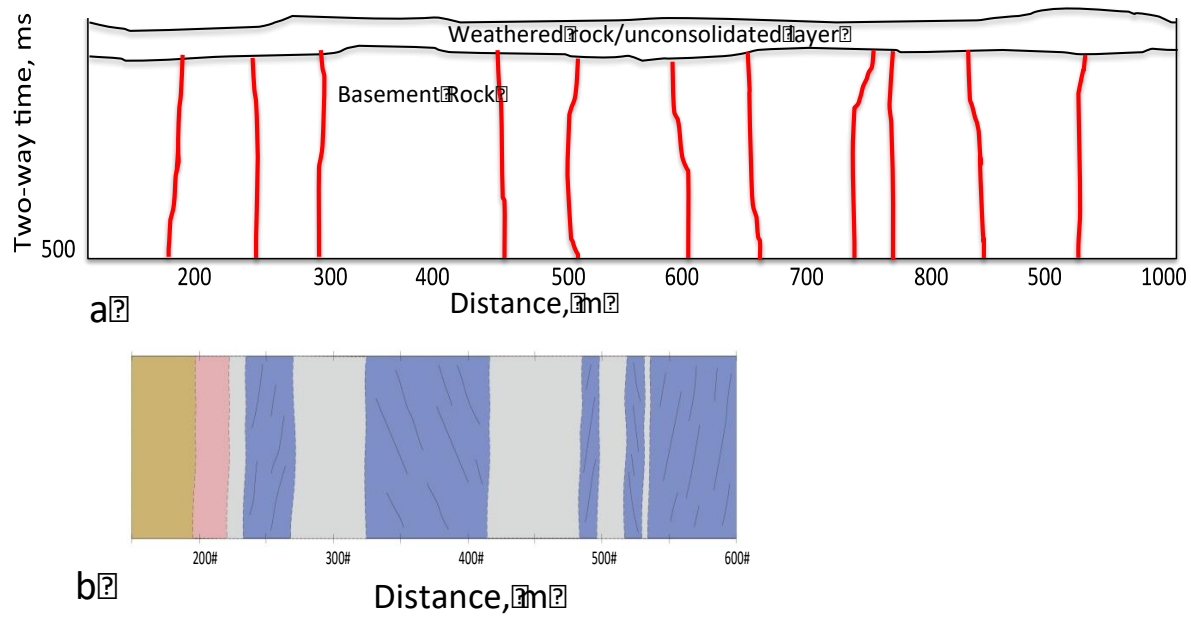

Figure 10: (a) cross section of the faults line interpreted from CDP-stacked seismic section, (b) cross section of the fault line projections from geological field mapping.

5. Conclusion

A combination of techniques employing the special attributes that distinguish primary reflections from other wave modes is used to process a set of ultra-shallow reflection data acquired in Elsaltador community, Southeastern Spain. The data has low signal-to-noise ratio is dominated by ground rolls and air waves faking reflection hyperbola. Careful validation of

primary reflections by synthetic modelling, application of amplitude based polygon muting, and $f - kx$ spectral filtering were used to decimate the non-reflection events. Optimum velocity for move-out correction was achieved by a combination of Constant Velocity Gather (CVG), Semblance Plot (SP), and Constant Velocity Stack (CVS). The stacked seismic section revealed weak lithological interface between the weathered layer and the faulted (mica-schist) basement rock and some vertical faults in the basement rock.

The weak interface is confirmed by synthetic modelling and explained by poor acoustic contrast between the weathered layer and the mica-schist basement rock. The weathered layer is made of about 15 ft (~ 5 m) thick unconsolidated low velocity profile unconformably lying on the mica-schist basement rock. The mica-schist reveals some minor faults with approximate northeast-southwest orientation. The presence of these faults is supported by independent geological field mapping.

Acknowledgements

The shallow reflection seismic data was acquired by a team of geophysicist at University of Liverpool led by Professor Andreas Rietbrock. Data acquisition was sponsored by a consortium. The Data was released to the author in 2011 for summer research. Many thanks to Professor Andreas Rietbrock, the acquisition team and the sponsor.

References

Baker, G. S., Steeples, D. W. and Drake, M. (1998): Muting the noise cone in near-surface reflection data: An example from southeastern Kansas. *Geophysics*. **63**, 1332-1338.

Black, R. A., Steeples, D. W. and Miller, R. D. (1994): Migration of shallow seismic-reflection data. *Geophysics*. **59**, 402-410.

Evison, F. F. (1952): The inadequacy of the standard seismic techniques for shallow surveying. *Geophysics*. **17**, P867-875.

Faulkner, D. R., Lewis, A. C. and Rutter, E. H. (2003): On the internal structure and mechanics of large strike - slip fault zone: field observations of the carboneras fault in Southeastern Spain. *Techtonophysics*. **367**, 235 - 251.

Gruber, W. and Rieger, R. (2003): High-resolution seismic reflection – Constraints and Pitfalls in groundwater exploration. *Materials and Geoenvironment*. **50**(1). 133-136.

Haberland, C., Maercklin, N., Kesten, D., Ryberg, T., Janssen, C., Agnon, A., Weber, M., Schulze, I. and El - Kelani, R. (2007): Shallow architechture of the Wadi Arabia fault (Dead Sea Transform) from high resolution seisic investigations. *Techtonophysics*. **423**, 37 - 50.

Hover, G. M. and O'Brien, J. T. (1980): The influence of planted geophones on seismic land data. *Geophysics*. **45**, 1239-1253.

Maercklin, N., Bedrosian, P. A., Haberland, C., Ritter, O., Ryberg, T., Weber, M. and Weckman, U. (2005): Characterising a large shear zone using seismic and magnetotelluric methods - the case of the dead sea transform. *Geophysical research letters*. **32**, L15303, doi: 10.1029/2005GL022724.

Miller, R. D. (1992): Normal moveout stretch mute on shallow- reflection data. *Geophysics*. **57**, 1502-1507.

Platt, J. P. and Whitehouse, M.J. (1999): Early Miocene high-temperature metamorphism and rapid exhumation in the Betic Cordillera (Spain): evidence from UePb zircon ages. *Earth and Planetary Science Letters*. **171**, 591 – 605.

Raji, W.O. And Rietbrock, A. (2013): Determination of Attenuation (1/Q) in Reflection Seismic Data. *Journal of Geophysics and Engineering***. 10**(4), 1-8 (045012).

Raji, W.O., Gao. Y. and Harris, J. M. (2015): Elastic wave field Simulation and Analysis for Cross Well Seismic Profiles. *NAPE Bulletin*. **27**, 42-51.

Raji, W. O., Harris, J. M. and Lu, S. (2016): Seismic velocity tomography for CO2 monitor in subsurface geological structures. *Journal of King Saud University–Science.* DOI:10.1016/j.jksus.2016.10.006.

Rutter, E. H., Faulkner, D. R. and Burgess, R. (2012): Structure and geological history of the Carboneras Fault Zone, SE Spain: Part of a stretching transform fault system. *Journal of structural Geology*. **45**, 68-86.

Steeples, D. W. and Richard, P. G. (1998): Avoiding pitfalls in shallow seismic reflection surveys. *Geophysics*. **63**, 1213-1224.

Yilmaz, O. (1980): *Seismic data processing. Society of Exploration Geophysics.* Tulsa Oklahoma. Pg. 285.